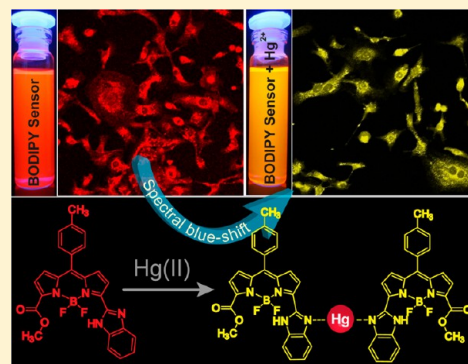


Sensing Hg(II) *in Vitro* and *in Vivo* Using a Benzimidazole Substituted BODIPYSheri Madhu,[†] Dharmendar Kumar Sharma,[†] Santanu Kumar Basu,[‡] Sameer Jadhav,[‡] Arindam Chowdhury,^{*,†} and Mangalampalli Ravikanth^{*,†}[†]Department of Chemistry and [‡]Chemical Engineering, Indian Institute of Technology Bombay, Powai, Mumbai 400 076, India

S Supporting Information

ABSTRACT: A multisignaling Hg(II) sensor based on a benzimidazole substituted BODIPY framework was designed, which displays excellent selectivity toward Hg(II) *in vitro* and *in vivo*. Optical and fluorogenic measurements in solution reveal that the sensor can detect mercury ions at submicromolar concentrations, with high specificity. The detection of Hg(II) is associated with a blue-shift in optical spectra and a simultaneous increase in the fluorescence quantum yield of the sensor, which is attributed to a decrease in charge delocalization and inhibition of photoinduced electron transfer upon binding to Hg(II). Using several spectroscopic measurements, it is shown that the binding mechanism involves two sensor molecules, where lone pairs of the benzimidazole nitrogen coordinate to a single mercury ion. The utility of this BODIPY sensor to detect Hg(II) *in vivo* was demonstrated by fluorescence imaging and spectroscopy of labeled human breast adenocarcinoma cells. While average emission intensity of the sensor over a large number of cells increases with incubated mercury concentrations, spatially resolved fluorescence spectroscopy performed on *individual cells* reveals clear spectral blue-shifts from a subensemble of sensors, corroborating the detection of Hg(II). Interestingly, the emission spectra at various submicrometer locations within cells exhibited considerable inhomogeneity in the extent of blue-shift, which demonstrates the potential of this sensor to monitor the local (effective) concentration of mercury ions within various subcellular environments.



■ INTRODUCTION

In spite of its toxicity, mercuric salts are widely used in industrial processes and products,¹ and as a consequence, high levels of mercury contamination have spread across the atmosphere and surface waters.² Mercury poses serious problems to human health, as bioaccumulation of mercury within the brain and kidneys ultimately leads to neurological diseases.³ Concern over its toxicity has stimulated explorations aimed at developing selective and efficient methods to monitor mercury in aqueous media, and by far, fluorescence based detection has emerged as a primary tool to do so.⁴ However, the development of practical fluorescent chemosensors for the Hg(II) ion still remains a challenge for several reasons: (i) Hg(II) being a heavy metal ion is known to quench fluorescence via enhanced spin-orbit coupling or energy/electron transfer,⁵ and (ii) although Hg(II) ions are relatively easy to chelate and detect in common organic solvents, they are rather difficult to recognize directly in aqueous environments due to the strong hydration energy of the sensors, which results in a lack of efficient detection of the analyte in biological (cellular) environments.⁶

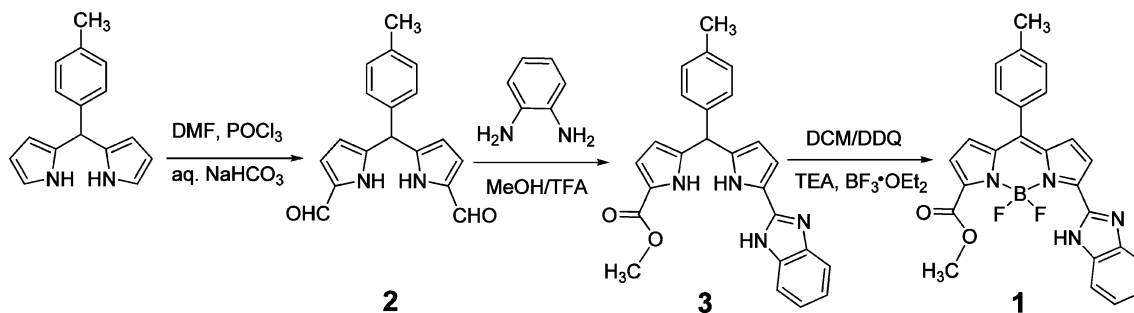
The methodology that most fluorogenic chemosensors rely on is emission intensity changes (quenching, enhancement, or ratiometric) of chromophore units which acts as reporters for sensory ability.⁷ Although systematic variations in emission

intensity can be related to the sensing capability for *in vitro* measurements, it is challenging to establish the detection of analytes inside biological cells (*in vivo*) because intensity can be altered for several other reasons as well. For instance, while imaging cells using fluorescence microscopy, quenching of emission can be misleading since many organic molecules used as sensors can photobleach⁸ and/or aggregate⁹ to various extents in different cellular environments. Further, unlike solution studies, the extent of labeling of the sensor at different locations within biological cells is often nonuniform, which can lead to diverse emission intensities at different spatial locations.¹⁰ These ambiguities can result in difficulty to deconvolute signal (intensity) changes due to sensing of analytes with those arising from sensor concentration fluctuations within cells. Therefore, it is imperative to (i) develop novel sensors which exhibit spectroscopic signatures other than just intensity changes, such as large spectral shifts, upon binding to analytes like Hg(II) and (ii) use techniques such as spatially resolved fluorescence spectroscopy to probe the response of sensors at different locations within individual cells. So far, there are only a few reports where sensors have been shown to exhibit a continuous increase of spectral shifts

Received: May 30, 2013

Published: September 25, 2013

Scheme 1. Synthesis of BODIPY 1



(transition energies) upon binding to Hg(II) ions in solution (*in vitro*).^{11,12} Furthermore, no attempt has been made to obtain emission spectra from a subensemble of sensors located in different cellular regions and test their analyte detection capability *in vivo*.

To perform the requisite study *in vivo*, a highly selective Hg(II) sensor is required which operates efficiently in aqueous (physiological) media and exhibits a systematic increase in both intensity as well as spectral shifts as a function of increasing analyte concentrations. This warrants rational design of a sensor with an optimal choice of electronically coupled fluorophore and receptor units, which can be generated using simple synthetic strategies. Most of the sensors used for the detection of Hg(II) consist of fluorophore and macrocyclic receptor units,^{4a-c,5c,6b,13} and it has been shown that for selective detection of Hg(II), nitrogen containing receptors are a good choice.¹⁴ Imidazole and benzimidazole possesses excellent hydrogen donor moieties like NH and pyridine-like nitrogen atom within the ring, which are useful for selective binding of anions and cations.¹⁵ Thus, imidazole and benzimidazole rings connected to fluorophores have received a lot of attention in recent times for their potential use as fluorescent sensors for the detection of heavy metal ions.¹⁶ Highly fluorescent boron-dipyrromethene (BODIPYs) dyes, with high extinction coefficients,¹⁷ narrow emission bandwidths, and stability toward light and chemicals, have emerged to be important for biological imaging.¹⁸ Besides, tunability of excitation/emission wavelengths of BODIPYs in the visible spectral range¹⁹ can be altered with relative ease by simple synthetic modifications of the dipyrromethene framework.²⁰ Therefore, novel properties of these two moieties (receptor and reporter) can be combined into a single molecular framework to generate a sensor in which the heavy metal-ion binding properties of benzimidazole can be monitored by following electronic structure changes of the BODIPY unit.

Interestingly, there are very few reports on BODIPY systems connected to imidazoles (or their derivatives), which were synthesized using imidazole substituted pyrroles.²¹ In this work, using a simple approach, we synthesized a benzimidazole substituted BODIPY sensor using 1,9-diformyl dipyrromethane as a key precursor,^{20b} such that the presence of benzimidazole at the three-position of the BODIPY significantly alters its electronic properties. We found that this molecule (designated BODIPY 1) is a multisignaling sensor *in vitro* and acts as an efficient and selective probe for Hg(II) in organic-aqueous solvent media, evidenced by various spectroscopic and electrochemical measurements. Remarkably, upon binding to Hg(II) in solution, both absorption and the emission spectra of BODIPY 1 display a dramatic blue-shift of transition energies in addition to an increase in the emission efficiency, which renders

it a good colorimetric and fluorogenic sensor. As a proof of principle for applicability of the designed sensor in biological systems, we have used spectrally resolved fluorescence microscopy to probe the detection of Hg(II) within individual human breast adenocarcinoma cells. This allowed us to investigate the spectral changes of the sensor upon mercury ion detection at different submicroscopic domains within cells and demonstrate its utility as a reporter for effective local concentrations of Hg(II) *in vivo*.

RESULTS AND DISCUSSION

Synthesis and Characterization of the Sensor. The desired benzimidazole substituted BODIPY 1 was synthesized as outlined in Scheme 1. BODIPY 1 was prepared in a stepwise approach starting with 1,9-diformyl dipyrromethane 2, which was condensed with *o*-phenylene diamine in methanol in the presence of a catalytic amount of TFA to generate compound 3. This was first oxidized with DDQ followed by neutralization with triethylamine and reacted with BF₃·OEt₂ to afford BODIPY 1. This molecule was characterized using various spectroscopic techniques, the details of which are provided in Figures S1–S7 of the Supporting Information (SI). Figure 1

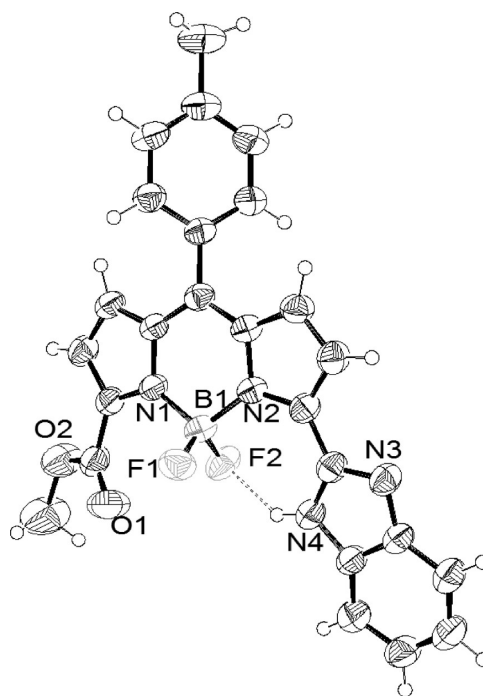


Figure 1. Molecular structure of BODIPY 1. Thermal ellipsoids are drawn at the 50% probability level.

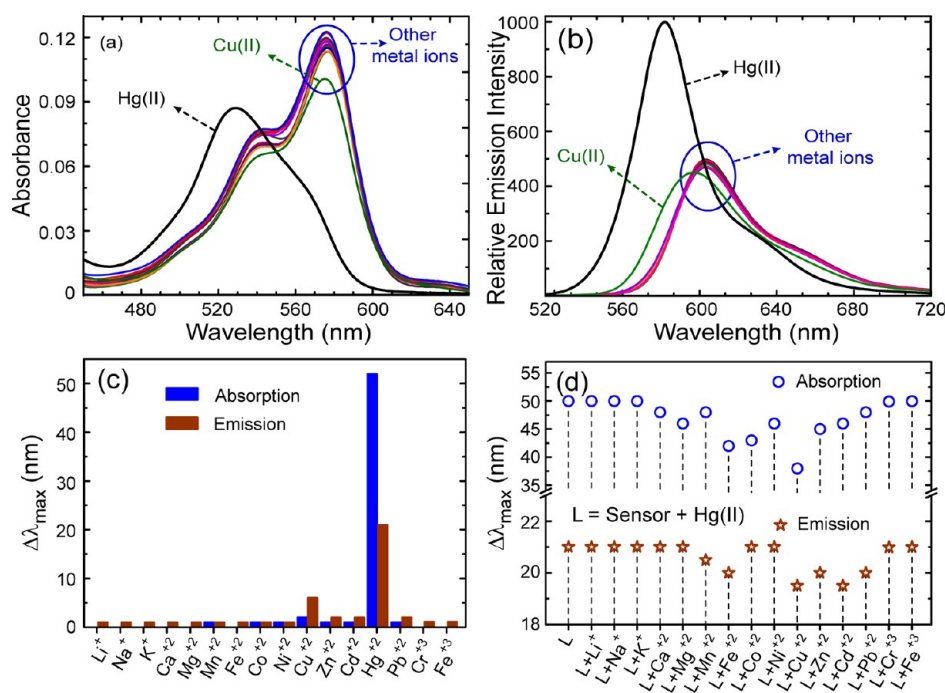


Figure 2. (a) Absorption and (b) emission spectra of BODIPY **1** ($1 \mu\text{M}$) upon the addition of different metal ions ($20 \mu\text{M}$) of (Li^+ , Na^+ , K^+ , Ca^{2+} , Mg^{2+} , Mn^{2+} , Fe^{2+} , Co^{2+} , Ni^{2+} , Cu^{2+} , Zn^{2+} , Cd^{2+} , Hg^{2+} , Pb^{2+} , Cr^{3+} , and Fe^{3+}) in $\text{CH}_3\text{CN}/\text{PBS}$ (7:3; v/v, pH 7.4) solution. (c) Bar chart depicting the extent of the blue-shift ($\Delta\lambda_{\text{max}}$) in absorption and emission peak positions in the absence and presence of various metal ions. (d) The extent of blue-shift in absorption and emission maxima ($\Delta\lambda_{\text{max}}$) of BODIPY **1** in the presence of $\text{Hg}(\text{II})$ upon the addition of excess amounts ($30 \mu\text{M}$) of various metal ions. $\text{L} = [\text{BODIPY } \mathbf{1} + \text{Hg}(\text{II})]$.

shows the X-ray crystal structure (CCDC 900420; Table S1, SI) of BODIPY **1**, where a planar BODIPY framework comprised of two pyrrole rings and a central six membered boron ring is observed. The striking feature of BODIPY **1** is the presence of intramolecular hydrogen bonding between fluoride atoms and the NH proton, which helps to keep the benzimidazole moiety and BODIPY core in one plane and, as a consequence, enables effective electronic communication between the BODIPY core and the benzimidazole units.

The electronic and optical properties of the designed sensor **1** were characterized by using UV–vis absorption as well as steady-state and time-resolved fluorescence spectroscopy. In an acetonitrile medium, BODIPY **1** shows an absorption peak position ($\lambda_{\text{max}}^{\text{Abs}}$) at 577 nm with a distinct shoulder at ~ 545 nm. The emission spectra is found to be reasonably narrow (line width $\sim 1200 \text{ cm}^{-1}$), with a maxima ($\lambda_{\text{max}}^{\text{Em}}$) located at 603 nm and a quantum yield of 0.42 (Figure S12 and Table S1, SI). Fluorescence lifetime measurements using time-correlated single photon counting (TCSPC) reveals that the singlet state of BODIPY **1** decays by following single-exponential kinetics with a lifetime of ~ 4.3 ns (Table S2, SI). Qualitatively similar behaviors of BODIPY **1** in terms of emission quantum yields and radiative lifetimes are observed in semiaqueous (water–acetonitrile) environments as well, pointing out to its potential as a fluorogenic reporter under physiological conditions. Therefore, all *in vitro* experiments for metal-ion sensing were performed in a 7:3 mixture (v/v) of acetonitrile/phosphate buffered saline (PBS), at pH 7.4.

Sensing $\text{Hg}(\text{II})$ *in Vitro*. The metal-ion recognition capability of BODIPY **1** was systematically carried out for diverse metal ions in $\text{CH}_3\text{CN}/\text{PBS}$ solution. First, using visual inspection, we checked for color changes of BODIPY **1** under both ambient and UV light, with the addition of the various

metal perchlorates (Li^+ , Na^+ , K^+ , Ca^{2+} , Mg^{2+} , Mn^{2+} , Fe^{2+} , Co^{2+} , Ni^{2+} , Cu^{2+} , Zn^{2+} , Cd^{2+} , Hg^{2+} , Cr^{3+} , and Fe^{3+}). It is found that a discernible color change (from pink to orange) of the BODIPY **1** solution occurs only in the presence of two metal ions, namely $\text{Cu}(\text{II})$ and $\text{Hg}(\text{II})$ (Figure S14, SI). However, the change of color due to the presence of $\text{Cu}(\text{II})$ was not as prominent as that for $\text{Hg}(\text{II})$, which indicates that BODIPY **1** has the potential to act as a sensor for mercury ions. This prompted us to further investigate the selectivity of BODIPY **1** for $\text{Hg}(\text{II})$ using various spectrophotometric techniques. Figure 2a shows the absorption spectra of **1** in the presence of all the aforesaid metal ions, which reveals a dramatic blue-shift ($\Delta\lambda_{\text{max}}^{\text{Abs}} > 50$ nm) of the entire absorption envelope only in the presence of $\text{Hg}(\text{II})$, consistent with the colorimetric assay. In addition, the fluorescence emission spectra (Figure 2b) of BODIPY **1** are found to be considerably altered in the presence of $\text{Hg}(\text{II})$, with a prominent blue-shift of transition energies ($\Delta\lambda_{\text{max}}^{\text{Em}} > 20$ nm) and a simultaneous increase of emission efficiency. It is noted that the emission spectrum remains unaltered in the presence of most other metal ions and shows a nominal $\Delta\lambda_{\text{max}}^{\text{Em}}$ of ~ 5 nm in Cu^{2+} solutions. The extent of the blue-shift of peak positions ($\Delta\lambda_{\text{max}}$) associated with various metal ion bindings of BODIPY **1** are plotted as a bar chart in Figure 2c. This shows remarkable changes in both the absorption and emission peak positions only in the presence of mercury ions, which portrays that BODIPY **1** acts as a highly selective sensor for the detection of $\text{Hg}(\text{II})$ in solution. Moreover, competitive binding experiments performed by the addition of excess amounts (30 equivalents) of other metal ions did not revert the spectral change induced due to $\text{Hg}(\text{II})$ binding (Figure 2d), which demonstrates that the sensor can specifically detect mercury ions even in the presence of other analyte ions.

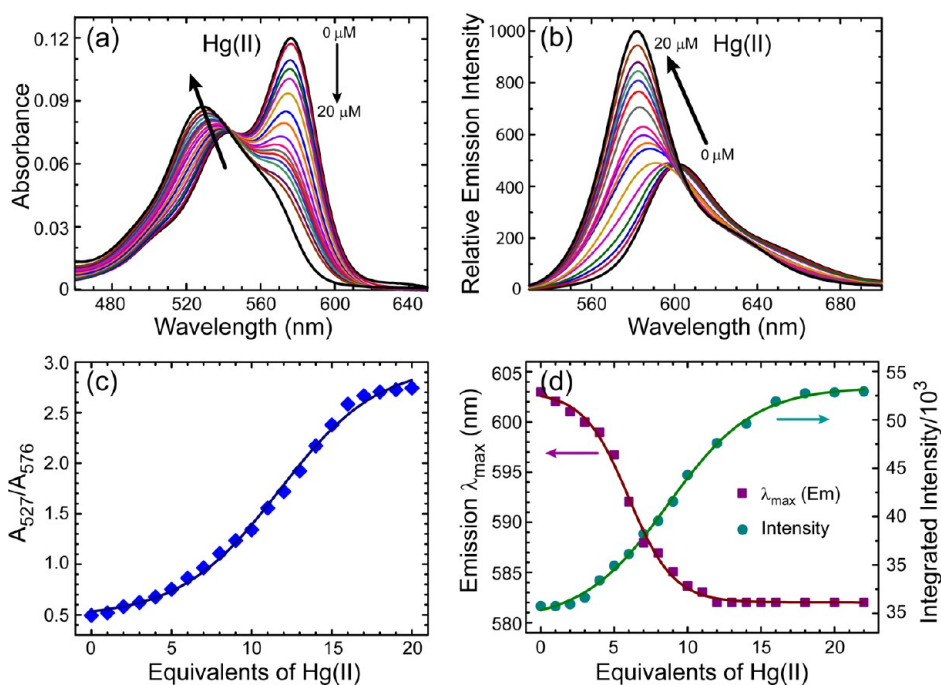


Figure 3. (a) Absorption and (b) fluorescence emission spectra of BODIPY 1 ($1 \mu\text{M}$) upon titration with Hg(II) ($\text{Hg}(\text{ClO}_4)_2$) in $\text{CH}_3\text{CN}/\text{PBS}$ (7:3; v/v, pH 7.4) solution. (c) Ratiometric response of the absorbance at 527 and 576 nm with increasing Hg(II) concentration. (d) Emission maxima (squares) and the integrated emission intensity (circles) of BODIPY 1 as a function of Hg(II) concentration and their corresponding best fits (solid lines) using a Boltzmann function.

The binding and detection of Hg(II) by BODIPY 1 was systematically studied by titration measurements using spectrophotometric assays. Figure 3a,b show the changes in absorption and fluorescence spectra of the sensor in $\text{CH}_3\text{CN}/\text{PBS}$ solution upon the addition of increasing amounts of mercury ions (0 to 20 equivalents). Figure 3a shows that with increasing Hg(II) concentration, the absorption band centered at 577 nm undergoes a continuous blue-shift with an isosbestic point at ~ 545 nm, suggesting interconversion of two species which we attribute to the free BODIPY 1 and the mercury ion bound sensor, respectively. The ratio of absorbance at 577 nm (for free sensor) and at 529 nm (for Hg(II) bound sensor) at different equivalents of Hg(II) is plotted in Figure 3c, the sigmoidal nature of which serves as an indicator of analyte binding. With increasing equivalents of Hg(II), the fluorescence emission spectra (Figure 3b) of the sensor also display a continuous blue-shift ($\lambda_{\text{max}}^{\text{Em}}$ changes from 603 to 582 nm) in conjunction with an increase in the emission quantum yield (Φ_f increased from 0.42 to 0.58). The analyses of the emission spectra with increasing Hg(II) concentrations are plotted in Figure 3d, in terms of the $\lambda_{\text{max}}^{\text{Em}}$ and integrated (relative) intensities. From the changes in fluorescence intensity, the binding constant for sensing Hg(II) in the mixed solvent was estimated to be $6.18 \times 10^6 \text{ M}^{-1}$ (Figure S15, SI) using the Benesi–Hildebrand equation. The sensitivity of BODIPY 1 for the Hg(II) ion has been further evaluated by measuring the lowest concentration of the analyte, using the linear dynamic response.²² The detection limit (LOD) was measured to be $0.77 \mu\text{M}$, suggesting its applicability of the sensor to detect Hg(II) even in the submicromolar range.

To understand the origin of the shift in transition energies of BODIPY 1 upon binding to Hg(II), we have performed electrochemical studies of the sensor in a $\text{CH}_3\text{CN}/\text{H}_2\text{O}$ medium. Using cyclic voltammetry, we found that BODIPY 1

undergoes two reversible reductions (Figure 4, inset) at ~ -0.475 and ~ -1.37 V, which indicates the electron deficient

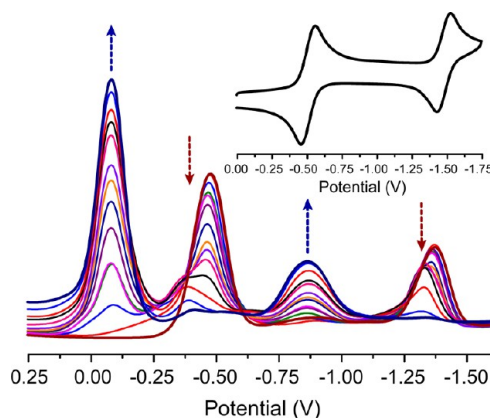


Figure 4. Square wave voltammogram of BODIPY 1 (10 mM) in the presence of different concentrations of Hg(II) solution (from 0 to 50 mM) in $\text{CH}_3\text{CN}/\text{PBS}$ (7:3; v/v) containing 0.1 M TBAP as a supporting electrolyte recorded at a 50 mV s^{-1} scan rate. The scans with 0 and 50 mM of Hg(II) are represented as thicker lines for clarity. Inset shows reduction waves of the cyclic voltammogram of BODIPY 1 in the absence of Hg(II).

nature of the BODIPY core. The changes in reduction potential of BODIPY 1 were further followed by titration with Hg(II) using square wave voltammetry (Figure 4). Upon the addition of increasing amounts of Hg(II) to a solution of BODIPY 1, the reduction waves at -0.475 and -1.37 V (red arrows) disappeared completely with the simultaneous emergence of new waves at ~ -0.082 and ~ -0.870 V (blue arrows). This significant anodic shift (~ 400 mV) in reduction potentials indicates that the electron density on the BODIPY core is

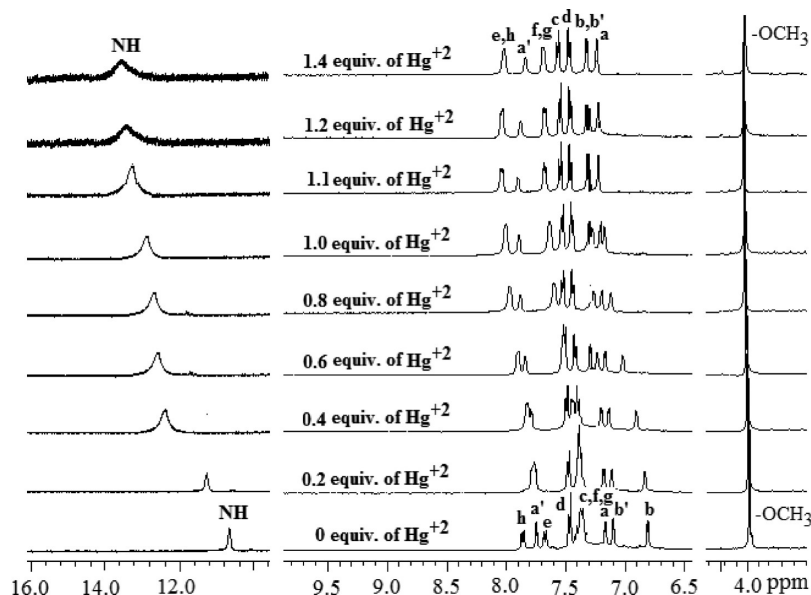


Figure 5. Partial ^1H NMR spectra of BODIPY **1** (16 mM) in 0.4 mL of $\text{CD}_3\text{CN}/\text{D}_2\text{O}$ (97.5:2.5, v/v) in the presence of increasing concentrations of $\text{Hg}(\text{II})$ in $\text{CD}_3\text{CN}/\text{D}_2\text{O}$. The (b,b') signals correspond to the pyrrole protons adjacent to the imidazole ring. The (a,a') signals correspond to pyrrole protons adjacent to the ester moiety. The (c,d) signals correspond to the aromatic protons of the *meso*-aryl ring, and the (e,f,g,h) signals correspond to the aromatic protons of the imidazole group (Scheme 2). The signal-to-noise ratio of the top three NH region NMR spectra is lower than the rest of the traces because of a pronounced metal-ion effect arising from a high concentration of $\text{Hg}(\text{II})$. To show that the N–H bond is intact after the addition of excess $\text{Hg}(\text{II})$, the NH signal for the top three spectra has been expanded vertically. All the signals were assigned on the basis of the correlations observed in the ^1H – ^1H COSY spectrum (Figure S7, Supporting Information).

further depleted upon binding with $\text{Hg}(\text{II})$ ions. This provides evidence that the fluorescence enhancement of BODIPY **1** upon $\text{Hg}(\text{II})$ binding is due to a blocking of photoinduced electron transfer (PET) from the benzimidazole nitrogen (donor) to the BODIPY unit (acceptor). Further, the electrochemical titration studies strongly suggest that binding of $\text{Hg}(\text{II})$ to the benzimidazole unit restricts the lone pair of nitrogen to participate in delocalization with the BODIPY core. As a consequence of the decreased amount of charge delocalization, the optical transitions of the mercury bound sensor occur at higher energies as compared to the free BODIPY **1** in solution.

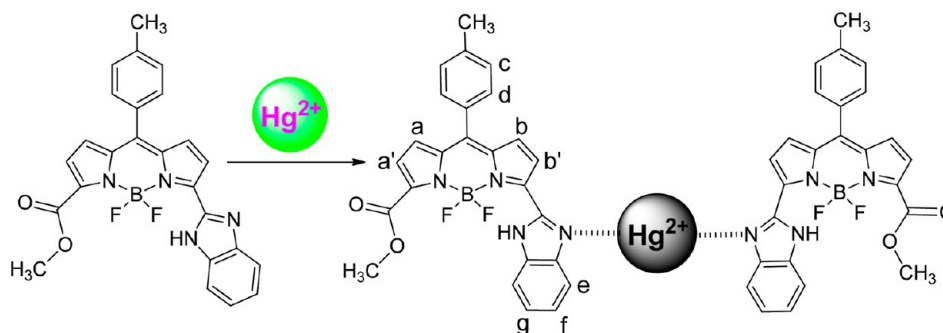
Electrochemical studies point out that the lone-pair of the benzimidazole nitrogen in BODIPY **1** is very likely to be involved in coordination to the $\text{Hg}(\text{II})$. To elucidate the binding mechanism, we have performed ^1H NMR titration experiments in $\text{CD}_3\text{CN}/\text{D}_2\text{O}$ by varying the $\text{Hg}(\text{II})$ concentration, the results of which are shown in Figure 5. Upon the addition of increasing equivalents of $\text{Hg}(\text{II})$ up to 1.4 equivalents, the pyrrole protons (*types b, b'*) adjacent to the benzimidazole moiety, as well as benzimidazole aromatic protons (*types e, f*) experienced a significant downfield shift, which suggests the involvement of benzimidazole nitrogen atoms in binding to $\text{Hg}(\text{II})$. In addition, not only do we find that the benzimidazole NH proton does not disappear but it rather experiences a very significant downfield shift (~ 3.5 ppm), indicating that only one of the benzimidazole nitrogens is involved in coordination with $\text{Hg}(\text{II})$. It is also clear from Figure 5 that the pyrrole protons (*types a, a'*) of the BODIPY skeleton did not display any significant shift, suggesting that the oxygen atoms of the ester moiety do not participate in the detection of $\text{Hg}(\text{II})$.

To support the above argument that only the nitrogen of benzimidazole coordinates to $\text{Hg}(\text{II})$, we have performed IR measurements on BODIPY **1**, in the absence and in the

presence of 10 equivalents of $\text{Hg}(\text{II})$. In the IR spectrum, BODIPY **1** showed characteristic bands for benzimidazolic N–H, C=N, and esteric C=O at 3437, 1574, and 1732 cm^{-1} , respectively, in addition to other bands (Figure S17, SI).²³ However, the IR spectra recorded for the BODIPY **1**– $\text{Hg}(\text{II})$ complex did not show any change for band positions except for C=N of the benzimidazole moiety, which shows a blue-shifted transition at 1613 cm^{-1} . This clearly indicates binding of $\text{Hg}(\text{II})$ to the C=N benzimidazole nitrogen atom (Figure S18, SI). In addition, the observed blue-shift in this transition essentially reflects the strengthening of the C=N bond in the presence of $\text{Hg}(\text{II})$. This can be explained by the inhibition of electronic delocalization around the benzimidazolic unit,²³ which reinforces our previous inference on the origin of the blue-shift in the electronic spectra upon analyte detection.

Further, we note that in the NMR titration, a significant shift of the N–H peak (Figure 5, left panel) occurs up to 0.4–0.6 equivalents of $\text{Hg}(\text{II})$, and subsequent addition of the analyte results in nominal continuous changes in the peak position. This suggests that more than a single BODIPY **1** molecule is likely to be involved in binding to one mercury ion. To determine the binding stoichiometry of the BODIPY **1**– $\text{Hg}(\text{II})$ adduct, spectrophotometric measurements were carried out in the presence of varying mole fractions of $\text{Hg}(\text{II})$ in an acetonitrile–water medium (Figure S19a,b, SI). Job's plot analyses of both changes in the absorbance and the fluorescence intensity reveal a maximum at ~ 0.6 , indicative of the formation of a 2:1 complex between BODIPY **1** and $\text{Hg}(\text{II})$.

On the basis of the NMR titration measurements, IR spectroscopy, and Job's plot analyses, we propose that the $\text{Hg}(\text{II})$ binding mechanism of BODIPY **1** involves two benzimidazole moieties, where the nitrogen lone pairs coordinate to a single $\text{Hg}(\text{II})$ ion in a linear geometry (Scheme 2). However, it is difficult to comment on whether the two

Scheme 2. Proposed Binding Mechanism of Hg(II) by BODIPY 1^a

^aThe labeling of the protons is explained in Figure 5.

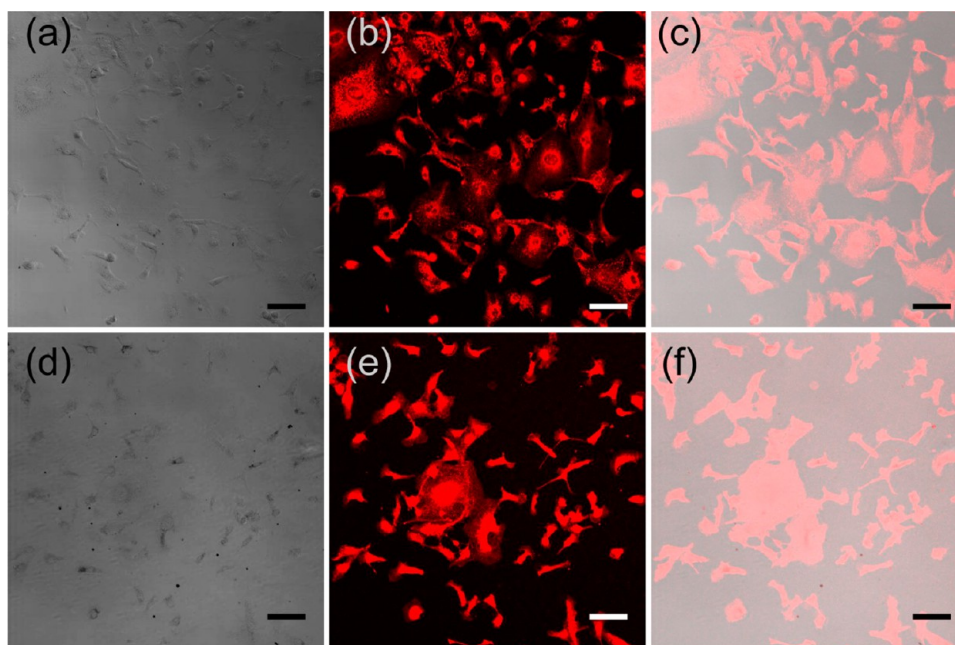


Figure 6. Cellular uptake of the BODIPY 1 by fixed MDA-MB-231 cells in the absence of Hg(II) (a–c) and after incubation with 10 μM of Hg(II) for 10 min (d–f). (a,d) Optical (DIC) images, (b,e) fluorescence (SCM) images, and (c,f) overlay of the DIC and fluorescence images of the same lateral area. Both the SCM fluorescence images were collected using the same emission filter (BP 560–615 nm) and depicted in pseudocolor, with brightness-contrast set at the same levels. Scale bar in the images is 100 μm .

BODIPY core units of the dimeric complex are syn- or anti- with respect to the N–Hg–N bond and if solvent molecules (water or acetonitrile) coordinate to the mercury ion and participate in complex formation. Nonetheless, to substantiate the proposed binding mechanism, we have performed mass spectrometry measurements (Figure S20, SI) in the presence of excess mercury ions using ESI-MS. The molecular ion peak at m/z of 1113.14 supports the formation of a 2:1 complex between BODIPY 1 and mercury (Figure S21, SI). Furthermore, the observed isotopic peak pattern was found to be in excellent agreement with those theoretically calculated for a dimeric complex (Figure S21 inset, SI), which reaffirms the proposed binding mechanism (Scheme 2) that imidazole nitrogen lone pairs from two BODIPY 1 molecules coordinate to a single mercury ion.

Spatially and Spectrally Resolved Sensing of Hg(II) *in Vivo*. To evaluate the feasibility for the application of BODIPY 1 as a mercury sensor inside cellular environments, as a test case, we have used the human breast adenocarcinoma cell line MDA-MB-231 for *in vivo* imaging measurements. In order to

check the cellular uptake of BODIPY 1, the living as well as fixed MDA-MB-231 cells were incubated for 20 min with varied concentrations of BODIPY 1 (see Materials and Methods) followed by visualization under an optical microscope. The DIC image of the fixed cells labeled with BODIPY 1 and the scanning confocal microscopy (SCM) image of the same lateral area obtained using 532 nm laser illumination are shown in Figure 6a,b. These images in conjunction with the overlay image (Figure 6c) show that the emission from BODIPY 1 arises from locations where the cells are present, and the emission intensities within the cells increase with increasing concentration of BODIPY 1 (data not shown). Similarly, in the presence of 10 μM Hg(II), the corresponding DIC, fluorescence, and overlay images of the BODIPY 1 labeled cells are shown in Figure 6d–f. It should be noted that the incubation time of Hg(II) was restricted to 10 min before fixing the cells, as the MDA-MB-231 cells start to round up after ~ 20 min due to mercury induced cell-death. Nonetheless, the sharp contrast in the fluorescence image (Figure 6b,e) indicates efficient cellular uptake of BODIPY 1, similar to other BODIPY

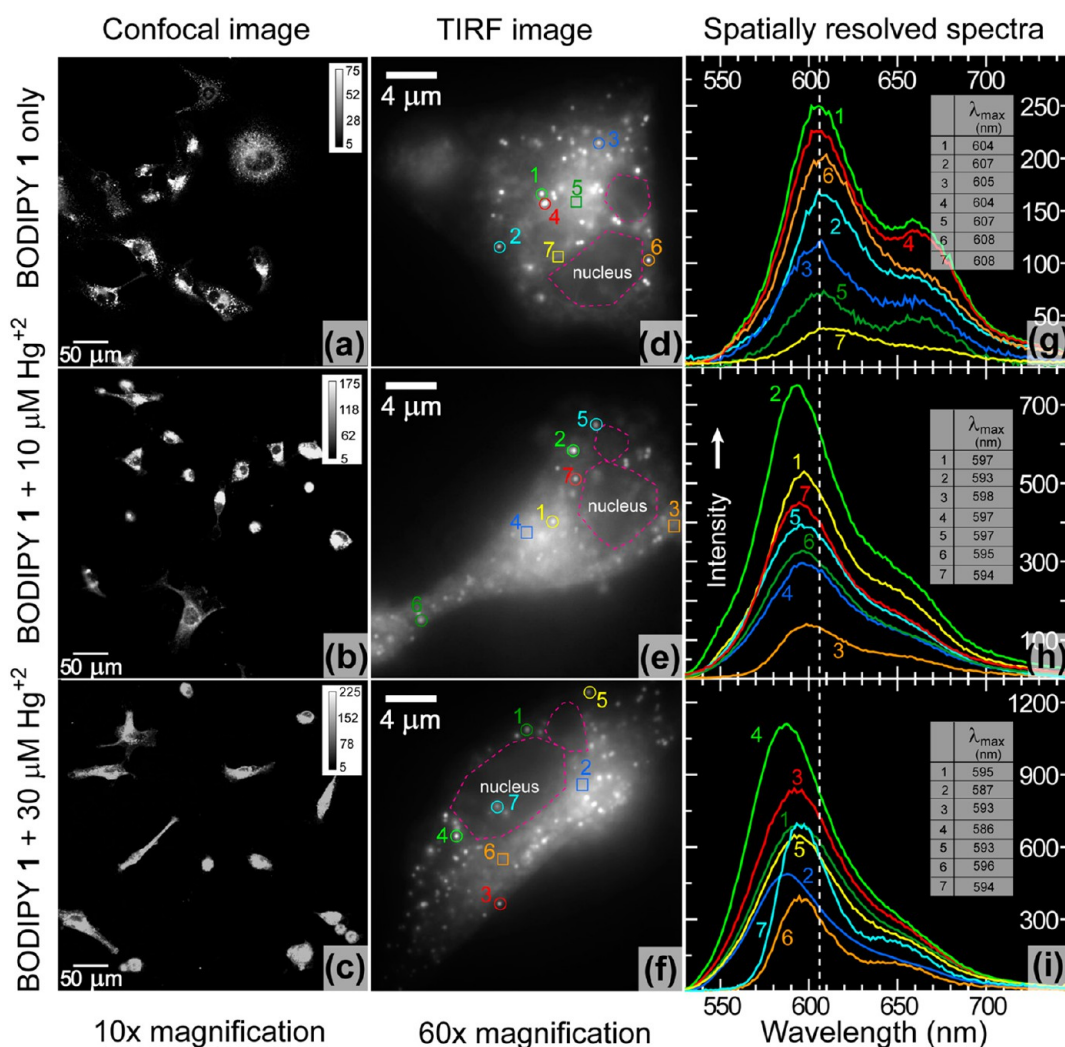


Figure 7. SCM images of BODIPY 1 ($1 \mu\text{M}$) labeled MDA-MB-231 cells in the absence (a) and presence of $10 \mu\text{M}$ (b) and $30 \mu\text{M}$ (c) of Hg(II) (incubation concentrations). Wide field TIRF images (d–f) displaying portions of single cells (nuclei shown with dotted lines) obtained from the same sample as in a–c. Representative fluorescence emission spectra (g–i) obtained from various local regions (marked with circles and squares) within each cell shown in d–f (regions marked 1–7), in the absence (g) and presence of $10 \mu\text{M}$ (h) and $30 \mu\text{M}$ (i) Hg(II) . The $\lambda_{\text{max}}^{\text{Em}}$ for each set of representative spatially resolved emission spectra are tabulated in the insets (g–i). The vertical line at 606 nm represents the average value of $\lambda_{\text{max}}^{\text{Em}}$ positions for 25 individual emission spectra in the absence of Hg(II) .

dyes used as cellular imaging agents.¹⁸ This demonstrates that BODIPY 1 can permeate through the cellular membrane for both live and fixed cells, which allowed us to test for its mercury sensing ability in cellular environments.

Fluorescence images of BODIPY 1 labeled cells in the absence and presence of different amounts of Hg(II) (0 , 10 , and $30 \mu\text{M}$ incubation for 10 min) are shown in Figure 7a–c. These SCM images show that the cytoplasm and cell membranes are preferentially labeled (in both the presence and absence of mercury), while the extent of BODIPY 1 penetration into the nuclei is considerably less as compared to rest of the cell. It is important to note that the fluorescence intensity of labeled cells, on average, increase by 3–4 fold in the presence of mercury ions (Figure 7a–c). Interestingly, closer inspection of individual cells via TIRF imaging (Figure 7d–f) reveals that BODIPY 1 is not uniformly distributed inside the cytoplasm; spatially separated bright emission spots are always observed on top of a weaker background emission (also seen in Figure 7b,e). Due to this spatial variation in emission intensity, from Figure 7d–f it is difficult to estimate the efficacy of

BODIPY 1 in the detection of mercury ions at different locations within cells. Therefore, it was imperative to obtain spatially resolved emission spectra to ascertain the sensory ability of BODIPY 1 in terms of spectral shifts associated with binding to Hg(II) . Figure 7g–i shows the fluorescence emission spectra obtained from seven different local regions within a single cell, in the absence and presence of mercury ions. These representative sets of spatially resolved emission spectra are only a few among several tens of spectra collected over various regions within a cell, as well as over different cells in the same sample.

Typically, in the absence of mercury ions, the spatially resolved emission spectra of BODIPY 1 show an emission maximum ($\lambda_{\text{max}}^{\text{Em}}$) at $\sim 606 \text{ nm}$ with a secondary peak (or a shoulder) between 650 and 670 nm , similar to that observed in ensemble studies (Figure 3b). In the presence of Hg(II) , the emission spectra of BODIPY 1 show a distinct blue-shift. For a Hg(II) concentration of $10 \mu\text{M}$, the average value of $\lambda_{\text{max}}^{\text{Em}}$ positions ($\bar{\lambda}_{\text{max}}$) is found to be $\sim 595 \text{ nm}$, while for higher concentrations ($30 \mu\text{M}$), the $\bar{\lambda}_{\text{max}}$ further shifts to $\sim 590 \text{ nm}$.

This blue-shift in transition energies serves as clear evidence that BODIPY 1 is able to detect the presence of mercury ions inside cells. In addition to spectral shifts, it is observed that the emission intensities of individual spectra in the presence of Hg(II) (Figure 7h–i) are generally higher as compared to those where no mercury is present (Figure 7g), in tune with the SCM intensity images (Figure 7a–c). Moreover, we found that the ratio (R) of emission intensities at the peak position (i.e., at $\lambda_{\text{max}}^{\text{Em}}$) and at $\lambda = 660$ nm computed from individual spectra, on an average, increases from 1.9 in the absence of mercury to 2.8 and to 3.4 for 10 and 30 μM Hg(II), respectively. This ratio, R , therefore serves as an additional measure of mercury ion sensing by BODIPY 1 within cellular environments.

Even though the $\lambda_{\text{max}}^{\text{Em}}$ positions show a clear blue-shift with a simultaneous increase in the intensity ratio (R) with increasing concentrations of mercury ions used to incubate the cells, there is considerable variation in both these parameters under all the conditions, i.e., at Hg(II) concentrations of 0, 10, and 30 μM . In the absence of mercury, the $\lambda_{\text{max}}^{\text{Em}}$ is found to range from 603 to 609 nm, while R values typically vary between 1.2 and 2.2. This fluctuation can be attributed to the variation in polarity of the local environment where BODIPY 1 resides, as well as to aggregation of the sensor in different cellular environments. In presence of 10 and 30 μM Hg(II) ions, we found that the $\lambda_{\text{max}}^{\text{Em}}$ (R values) obtained from different local regions' ranges between 591 and 600 nm (1.8–3.2) and 584 and 598 nm (2.3–4.4), respectively. This indicates that neither the extent of the blue-shift nor the R values solely depend on the amount of mercury used to incubate the cells. Rather, both of these parameters are extremely sensitive to the region of the cytoplasm from which each spectrum is obtained. It is therefore reasonable to conclude that the extent of blue-shift (as well as variation of R) is a consequence of inhomogeneity in the effective Hg(II) concentrations within the cells. This essentially demonstrates the ability of BODIPY 1 to effectively act as a local sensor of Hg(II) within cellular environments.

CONCLUSIONS

In conclusion, we have developed a new multisignaling sensor based on benzimidazole substituted BODIPY, which shows remarkable selectivity and specificity toward Hg(II) under physiological conditions. The sensory ability of BODIPY 1 was tested using several techniques, and it was found that this molecule serves as a very efficient optical sensor for Hg(II) with a submicromolar analytical detection capability. Interestingly, the optical spectra of BODIPY 1 undergo a continuous blue-shift in addition to an increase in the emission efficiency upon analyte detection. Such a shift in transition energies results in a color change from fluorescent pink to orange in response to Hg(II). Competitive binding experiments in the presence of various biologically relevant metal ions demonstrate that BODIPY 1 can specifically detect mercury ions *in vitro*. Electrochemical studies reveal that the blue shift in transition energies and simultaneous increase in emission efficiency upon Hg(II) binding is due to a depletion of charge delocalization on the BODIPY core and blocking of photoinduced electron transfer from imidazole nitrogen to the BODIPY unit. ^1H NMR titration experiments and a Job's plot analysis reveals that Hg(II) binding involves formation of a complex where imidazole nitrogens of two BODIPY 1's coordinate to a single mercury ion, the existence of which was confirmed by mass spectrometry. The utility of the sensor for detection of Hg(II) in biological systems was demonstrated by labeling human

breast adenocarcinoma cells with BODIPY 1 and investigating changes in emission intensity and shift in transition energies with different amounts of mercury ions. Confocal microscopy reveals that the fluorescence intensity of labeled cells increases on an average with increasing concentration of incubated mercury ions, even though the concentration of the sensor within the cell was not uniform. Spatially resolved emission spectroscopy measurements performed on individual cells reveal diverse shifts in transition energies in various submicrometer regions within each cell, clearly pointing out to the inhomogeneity in local mercury concentrations. Therefore, these measurements demonstrate not only that BODIPY 1 can be used to monitor the effective mercury concentrations within cellular environments but also the applicability of spectrally resolved fluorescence imaging in detection of analytes *in vivo*.

MATERIALS AND METHODS

Chemicals. The chemicals such as $\text{BF}_3 \cdot \text{Et}_2\text{O}$ and 2,3-dichloro-5,6-dicyano-1,4-benzoquinone (DDQ) were used as obtained from Aldrich. All other chemicals used for the synthesis were reagent grade, and solvents were dried by routine procedures immediately before use. Column chromatography was performed on silica gel (60–120 mesh).

Instrumentation. All the NMR spectra were recorded with a Bruker 400 MHz instrument using tetramethylsilane ($\text{Si}(\text{CH}_3)_4$) as an internal standard. Single-crystal X-ray diffraction data were collected on a charge-coupled-device (CCD) diffractometer with a liquid nitrogen vapor cooling device. Data were collected at 150 K with graphite-monochromatized Mo $K\alpha$ X-ray radiation ($\lambda = 0.71073$ Å). The structure was solved by direct methods and refined by full matrix least-squares against F^2 with all reflections. Non-hydrogen atoms were refined anisotropically. Additional details of the structure determinations for the BODIPY 1 can be found in the Supporting Information. Absorption and steady state fluorescence spectra were obtained with Perkin-Elmer Lambda-35 and Varian Cary-Eclipse ($\lambda_{\text{ex}} = 500$ nm, excitation and emission slit widths = 2.5 nm) instruments, respectively. The elemental analyses were performed on a ThermoQuest microanalysis instrument. FT-IR spectra were measured on a Perkin-Elmer spectrometer using KBr pellets. Square Wave Voltammetric (SWV) studies were carried out with a BAS electrochemical system utilizing the three electrode configuration consisting of a glassy carbon (working electrode), platinum wire (auxiliary electrode), and saturated calomel (reference electrode) electrodes. The experiments were done in dry acetonitrile using 0.1 M tetrabutylammonium perchlorate (TBAP) as a supporting electrolyte. The time-resolved fluorescence decay measurements were carried out at the magic angle using a picosecond diode laser based time-correlated single photon counting (TCSPC) fluorescence spectrometer from IBH, U. K. The mass spectra were recorded on a Q-TOF micromass (YA-105) using the electrospray ionization method. For UV–vis and fluorescence titration experiments, the stock solution of BODIPY 1 (1 μM) was prepared by using spectroscopic grade $\text{CH}_3\text{CN}/\text{PBS}$ (7:3; v/v, pH 7.4), and $\text{Hg}(\text{ClO}_4)_2$ solution was prepared (5×10^{-4} M) in CH_3CN . The association constant of the mercury complex formed in solution has been estimated by using the standard Benesi–Hildebrand equation. The limit of detection (LOD) for the Hg(II) was calculated as 3 times the standard deviation for the average measurements of 10 blank samples by slope ($\text{LOD} = 3\sigma/K$).²² For ^1H NMR titration, a solution of BODIPY 1 in 0.4 mL of $\text{CD}_3\text{CN}/\text{D}_2\text{O}$ (97.5:2.5, v/v) was prepared (16 mM), and a 0.4-mL portion of this solution was transferred to a 5-mm NMR tube. A small aliquot of $\text{Hg}(\text{ClO}_4)_2$ in CD_3CN (160 mM) was added in an incremental fashion, and their corresponding spectra were recorded. Further details are provided in the Supporting Information.

Animal Cell Studies. *Materials.* Dulbecco's Modified Eagle's Medium (DMEM) [catalogue no. AL007A], fetal bovine serum (FBS) [catalogue no. RM1112], PBS without calcium and magnesium

[catalogue no. TL1006], trypsin-EDTA [catalogue no. TCL007], penicillin-streptomycin [catalogue no. A001A], and paraformaldehyde [catalogue no. RM3660] were obtained from HiMedia Laboratories, Mumbai, India.

Cell Culture. MDA-MB-231 human breast adenocarcinoma cells were obtained from the National Centre for Cell Science, Pune, India and were cultured in complete medium at 37 °C under a 5% CO₂ atmosphere. The complete medium was comprised of DMEM supplemented with 10% FBS and 1% antibiotics. For the experiments, after trypsinization, cells were seeded onto glass bottomed Petri dishes at a density of 5000 cells per square cm and incubated overnight.

Confocal Microscopy. For fluorescence imaging of living cells, 1 μ L of BODIPY 1 (1 mM) was added to the medium of the cells, and this was incubated for 20 min. Thereafter, DMEM was removed from the Petri dish, cells were washed twice with PBS (pH = 7.4), and fresh DMEM was added. For imaging of fixed cells, without Hg(II), these cells were fixed with 4% paraformaldehyde for 15–20 min, followed by incubation of the cells with 1 μ L of 1 mM BODIPY 1 in 1 mL of DMEM for 20 min. Then the cells were washed with PBS twice, and the fresh medium was added before performing optical microscopic measurement. For the detection of Hg(II) using BODIPY 1 in culture medium, MDA-MB-231 cells were incubated with 0 (without Hg), 10, and 30 μ L of 1 mM Hg(II) in 1 mL of DMEM for 10 min. Just before they rounded up (within \sim 15 min), the cells were fixed with 4% paraformaldehyde for 15–20 min. This was followed by incubation of all three samples [Hg²⁺ 0, 10, and 30 μ L] with BODIPY 1 (1 μ L of 1 mM) washed twice with PBS before optical imaging. The cells were visualized under a scanning confocal microscope (Carl Zeiss LSM 510) capable of taking DIC and fluorescence images of the same projected area using an excitation wavelength of 543 nm and an emission band-pass (BP) of 560–615 nm. The images were taken in both DIC and fluorescence format, the latter being represented in red pseudocolor (i.e., does not represent actual color of emission). The same samples were used for high resolution fluorescence imaging and spatially resolved spectroscopic measurements. The SCM images of labeled cells in the TOC graphic are represented in false colors to convey the blue-shift in emission spectra.

Spatially Resolved Fluorescence Spectroscopy. A home-built through-the-objective total internal reflection fluorescence (TIRF) microscopy setup based on an inverted optical microscope (Nikon TE2000U) was used to perform fluorescence imaging and obtain spatially resolved emission spectra. Details of the experimental setup are provided elsewhere.²⁴ In short, a 532 nm DPSS laser (30 mW) was used to excite the sample via a 1.49 NA 60 \times objective (Nikon, Apo TIRF). Typically, \sim 1 mW excitation powers were used to illuminate a \sim 30 \times 30 μ m² area of the sample. The fluorescence emission was collected using the same objective and passed through a dichroic mirror and emission filters (Semrock) and eventually imaged through a cooled interline CCD camera (DVC 1412AM). Spatially resolved emission spectra were obtained from different local regions (0.25 μ m²) of fixed cells using a combination of an adjustable slit and a transmission grating (300 g/mm) placed in front of the CCD in order to obtain both images and spectra simultaneously. The emission spectra were corrected for the CCD response and calibrated with several laser lines, resulting in a wavelength resolution of \sim 3 nm. All spectral data were obtained at identical excitation powers (\sim 400 W/cm²) and exposure times (500 ms). All the measurements are carried out at 295 K. All the experimental data were analyzed using freely available ImageJ (NIH) and Origin 7.5.

■ ASSOCIATED CONTENT

● Supporting Information

Experimental procedures, spectral data for the synthesis of new compounds, X-ray crystallographic data (CIF) for BODIPY 1, and spectroscopic data related to mercury(II) sensing. This material is available free of charge via the Internet at <http://pubs.acs.org>

■ AUTHOR INFORMATION

Corresponding Authors

*E-mail: arindam@chem.iitb.ac.in.

*E-mail: ravikanth@chem.iitb.ac.in.

Notes

The authors declare no competing financial interest.

■ ACKNOWLEDGMENTS

M.R. thanks the Department of Science and Technology (India) for financial support and A.C. acknowledges the Council of Scientific and Industrial Research (India) for a research grant (Scheme: 80(0070)/08/EMR-II). S.M. and D.K.S. acknowledge IIT Bombay and CSIR (India) for Ph.D. fellowships. The authors also thank the National Single-Crystal X-ray Diffraction Facility at IIT Bombay.

■ REFERENCES

- (1) (a) *Mercury Study Report to Congress*, EPA-452/R-97-003; United States Environmental Protection Agency, Office of Air Quality Planning & Standards and Office of Research and Development: Research Triangle Park, NC, 1997. (b) *Elemental Mercury and Inorganic Mercury Compounds: Human Health Aspects*; World Health Organization: Geneva, Switzerland, 2003.
- (2) (a) Fitzgerald, W. F.; Engstrom, D. R.; Mason, R. P.; Nater, E. A. *Environ. Sci. Technol.* **1998**, *32*, 1–7. (b) Zhuang, Y.; Thompson, J. S.; Zygarić, C. J.; Pavlish, J. *Environ. Sci. Technol.* **2004**, *38*, 5803–5808. (c) Kaim, W.; Schwederski, B. *Bioinorganic Chemistry: Inorganic Elements in the Chemistry of Life, an Introduction and Guide*; Wiley-Interscience: New York, 1991.
- (3) (a) Benoit, J. M.; Fitzgerald, W. F.; Damman, A. W. *Environ. Res.* **1998**, *78*, 118–133. (b) Boening, D. W. *Chemosphere* **2000**, *40*, 1335–1351. (c) Harris, H. H.; Pickering, I. J.; George, G. N. *Science* **2003**, *301*, 1203–1203.
- (4) (a) Descalzo, A. B.; Martínez-Mañez, R.; Radeaglia, R.; Rurack, K.; Soto, J. *J. Am. Chem. Soc.* **2003**, *125*, 3418–3419. (b) Zhang, X.-B.; Guo, C.-C.; Li, Z.-Z.; Shen, G.-L.; Yu, R.-Q. *Anal. Chem.* **2002**, *74*, 821–825. (c) Chen, C.-T.; Huang, W.-P. *J. Am. Chem. Soc.* **2002**, *124*, 6246–6247.
- (5) (a) McClure, D. S. *J. Chem. Phys.* **1952**, *20*, 682–686. (b) Varnes, A. W.; Dodson, R. B.; Wehry, E. L. *J. Am. Chem. Soc.* **1972**, *94*, 946–950. (c) Rurack, K.; Kollmannsberger, M.; Resch-Genger, U.; Daub, J. *J. Am. Chem. Soc.* **2000**, *122*, 968–969.
- (6) (a) Klein, G.; Kaufmann, D.; Schürch, S.; Reymond, J.-L. *Chem. Commun.* **2001**, 561–562. (b) Prodi, L.; Bargossi, C.; Montalti, M.; Zaccheroni, N.; Su, N.; Bradshaw, J. S.; Izatt, R. M.; Savage, P. B. *J. Am. Chem. Soc.* **2000**, *122*, 6769–6777.
- (7) (a) Nolan, E. M.; Lippard, S. J. *J. Am. Chem. Soc.* **2003**, *125*, 14270–14271. (b) Atilgan, S.; Ozdemir, T.; Akkaya, E. U. *Org. Lett.* **2010**, *12*, 4792–4795. (c) Sessler, J. L.; Davis, J. M. *Acc. Chem. Res.* **2001**, *34*, 989–997. (d) Michel, B. W.; Lippert, A. R.; Chang, C. J. *J. Am. Chem. Soc.* **2012**, *134*, 15668–15671.
- (8) (a) Giloh, H.; Sedat, J. W. *Science* **1982**, *217*, 1252–1255. (b) Sinnecker, D.; Voigt, P.; Hellwig, N.; Schaefer, M. *Biochemistry* **2005**, *44*, 7085–7094. (c) Henderson, J. N.; Ai, H.-W.; Campbell, R. E.; Remington, S. J. *Proc. Natl. Acad. Sci. U. S. A.* **2007**, *104*, 6672–6677. (d) Periasamy, N.; Bicknese, S.; Verkman, A. S. *Photochem. Photobiol.* **1996**, *63*, 265–271.
- (9) (a) Kaiser, T. E.; Stepanenko, V.; Würthner, F. *J. Am. Chem. Soc.* **2009**, *131*, 6719–6732. (b) Wang, K.-R.; Guo, D.-S.; Jiang, B.-P.; Sun, Z.-H.; Liu, Y. *J. Phys. Chem. B* **2010**, *114*, 101–106. (c) Zhao, Q.; Zhang, S.; Liu, Y.; Mei, J.; Chen, S.; Lu, P.; Qin, A.; Ma, Y.; Sun, J. Z.; Tang, B. Z. *J. Mater. Chem.* **2012**, *22*, 7387–7394.
- (10) (a) Qian, F.; Zhang, C.; Zhang, Y.; He, W.; Gao, X.; Hu, P.; Guo, Z. *J. Am. Chem. Soc.* **2009**, *131*, 1460–1468. (b) Hirayama, T.; Okuda, K.; Nagasawa, H. *Chem. Sci.* **2013**, *4*, 1250–1256. (c) Qian, Y.; Karpus, J.; Kabil, O.; Zhang, S.-Y.; Zhu, H.-L.; Banerjee, R.; Zhao, J.; He, C. *Nat. Commun.* **2011**, *2*, 495. (d) Jung, H. S.; Kwon, P. S.; Lee, J.

W.; Kim, J.; Hong, C. S.; Kim, J. W.; Yan, S.; Lee, J. H.; Joo, T.; Kim, J. *S. J. Am. Chem. Soc.* **2009**, *131*, 2008–2012.

(11) (a) Hatai, J.; Pal, S.; Jose, G. P.; Bandyopadhyay, S. *Inorg. Chem.* **2012**, *51*, 10129–10135. (b) Wu, Y.; Jing, H.; Dong, Z.; Zhao, Q.; Wu, H.; Li, F. *Inorg. Chem.* **2011**, *50*, 7412–7420. (c) Nasir, M. S.; Fahrni, C. J.; Suh, D. A.; Kolodnick, K. J.; Singer, C. P.; O'Halloran, T. V. *J. Biol. Inorg. Chem.* **1999**, *4*, 775–783.

(12) (a) Nolan, E. M.; Lippard, S. J. *J. Am. Chem. Soc.* **2007**, *129*, 5910–5918. (b) Chen, L.; Yang, L.; Li, H.; Gao, Y.; Deng, D.; Wu, Y.; Ma, L.-J. *Inorg. Chem.* **2011**, *50*, 10028–10032. (c) Coskun, A.; Akkaya, E. U. *J. Am. Chem. Soc.* **2006**, *128*, 14474–14475. (d) Taki, M.; Akaoka, K.; Iyoshi, S.; Yamamoto, Y. *Inorg. Chem.* **2012**, *51*, 13075–13077.

(13) (a) Yoon, J.; Ohler, N. E.; Vance, D. H.; Aumiller, W. D.; Czarnik, A. W. *Tetrahedron Lett.* **1997**, *38*, 3845–3848. (b) Cha, N. R.; Kim, M. Y.; Kim, Y. H.; Choe, J.-I.; Chang, S.-K. *J. Chem. Soc., Perkin Trans. 2* **2002**, 1193–1196. (c) Rurack, K.; Resch-Genger, U.; Bricks, J. L.; Spieles, M. *Chem. Commun.* **2000**, 2103–2104.

(14) Lehn, J.-M.; Montavon, F. *Helv. Chim. Acta* **1978**, *61*, 67.

(15) (a) Molina, P.; Tàrraga, A.; Otón, F. *Org. Biomol. Chem.* **2012**, *10*, 1711–1724. (b) Mazik, M.; Kuschel, M. *Chem.—Eur. J.* **2008**, *14*, 2405–2419. (c) Akhrif, Y.; Server, J.-C.; Sancho, A.; García, J.-L.; Escrivá, E.; Soto, L. *Inorg. Chem.* **2001**, *40*, 6832–6840. (d) Núñez, H.; Soto, L.; Server-Carrió, J.; García-Lozano, J.; Sancho, A.; Acerete, R.; Escrivá, E. *Inorg. Chem.* **2005**, *44*, 4644–4655.

(16) (a) Yoon, J.; Kim, S. K.; Singh, N. T.; Kim, K. S. *Chem. Soc. Rev.* **2006**, *35*, 355–360. (b) Xu, Z.; Kim, S. K.; Yoon, J. *Chem. Soc. Rev.* **2010**, *39*, 1457–1466. (c) Caballero, A.; White, N. G.; Beer, P. D. *Angew. Chem., Int. Ed.* **2011**, *50*, 1845–1848. (d) Gale, P. A. *Chem. Soc. Rev.* **2010**, *39*, 3746–3771.

(17) (a) Loudet, A.; Burgess, K. *Chem. Rev.* **2007**, *107*, 4891–4932. (b) Ulrich, G.; Ziessel, R.; Harriman, A. *Angew. Chem., Int. Ed.* **2008**, *47*, 1184–1201. (c) Boens, N.; Leen, V.; Dehaen, W. *Chem. Soc. Rev.* **2012**, *41*, 1130–1172.

(18) (a) Domaille, D. W.; Zeng, L.; Chang, C. J. *J. Am. Chem. Soc.* **2010**, *132*, 1194–1195. (b) Dodani, S. C.; Leary, S. C.; Cobine, P. A.; Winge, D. R.; Chang, C. J. *J. Am. Chem. Soc.* **2011**, *133*, 8606–8616. (c) Sun, Z.-N.; Wang, H.-L.; Liu, F.-Q.; Chen, Y.; Tam, P. K. H.; Yang, D. *Org. Lett.* **2009**, *11*, 1887–1890.

(19) (a) Olivier, J.-H.; Haefele, A.; Retailleau, P.; Ziessel, R. *Org. Lett.* **2010**, *12*, 408–411. (b) Nepomnyashchii, A. B.; Cho, S.; Rossky, P. J.; Bard, A. J. *J. Am. Chem. Soc.* **2010**, *132*, 17550–17559. (c) Murtagh, J.; Frimannsson, D. O.; O'Shea, D. F. *Org. Lett.* **2009**, *11*, 5386–5389. (d) Palma, A.; Alvarez, L. A.; Scholz, D.; Frimannsson, D. O.; Grossi, M.; Quinn, S. J.; O'Shea, D. F. *J. Am. Chem. Soc.* **2011**, *133*, 19618–19621. (e) He, H.; Lo, P.-C.; Yeung, S.-L.; Fong, W.-P.; Ng, D. K. P. *Chem. Commun.* **2011**, *47*, 4748–4750.

(20) (a) Buyukcikir, O.; Bozdemir, O. A.; Kolemen, S.; Erbas, S.; Akkaya, E. U. *Org. Lett.* **2009**, *11*, 4644–4647. (b) Madhu, S.; Rao, M. R.; Shaikh, M. S.; Ravikanth, M. *Inorg. Chem.* **2011**, *50*, 4392–4400. (c) Cakmak, Y.; Akkaya, E. U. *Org. Lett.* **2009**, *11*, 85–88. (d) Thivierge, C.; Loudet, A.; Burgess, K. *Macromolecules* **2011**, *44*, 4012–4015.

(21) (a) Noens, N.; Qin, W.; Baruah, M.; Borggraeve, W. M. D.; Filrowski, A.; Smisdon, N.; Ameloot, M.; Crovetto, L.; Talaveira, E. M.; Alvarez-Pez, J. M. *Chem.—Eur. J.* **2011**, *17*, 10924–10934. (b) Poronik, Y. M.; Yakubovskiy, V. P.; Shandura, M. P.; Vlasenko, Y. G.; Chernega, A. N.; Kovtun, Y. P. *Eur. J. Org. Chem.* **2010**, 2746–2752.

(22) (a) Cao, C.; Kim, J. P.; Kim, B. W.; Chae, H.; Yoon, H. C.; Yang, S. S.; Sim, S. J. *Biosens. Bioelectron.* **2006**, *21*, 2106–2113.

(23) (a) Sun, Q.; Yan, B. *Bioorg. Med. Chem. Lett.* **1998**, *8*, 361–365. (b) Mohan, S.; Sundaraganesan, N. *Spectrochim. Acta.* **1991**, *47*, 1111–1115.

(24) (a) De, S.; Layek, A.; Raja, A.; Kadir, A.; Gokhale, M. R.; Bhattacharya, A.; Dhar, S.; Chowdhury, A. *Adv. Funct. Mater.* **2011**, *21*, 3828–3835.